Validating DLO models from shape observation

Validating DLO Models from Shape Observation

Gianluca Palli[b], Salvatore Pirozzi[a]

***Abstract*—In this paper, the problem of fitting the model of deformable linear objects from the observation of the shape under the effect of known external forces like gravity is taken into account. The model of the deformable linear object is based on dynamic splines, allowing to obtain a reliable prediction of the object behavior while preserving a suitable efficiency and simplicity of the model. The object shape is measured by means of a calibrated vision system, and a fitting between the observed shape and the theoretical model is defined for validation. Experiments are executed in different conditions, showing the reliability of the proposed spline-based model.**

***Index Terms*—Model Identification, Parameter Estimation, Deformable Linear Objects, Robotic Manipulation**

I. Introduction

The manipulation of deformable objects plays a relevant role in the implementation on novel manufacturing applications in several sectors, ranging from food production [1] to textile manufacturing [2], surgery [3], automotive [4], aerospace [5] and electromechanical industries [6] in general. In industrial scenarios, many assembly operations involving deformable objects are still executed manually due to the variability of initial configurations and unpredictable behaviors of the objects. A thoughtful survey on robotic manipulation of deformable objects in domestic and industrial applications can be found in [7].

A particularly relevant subfield of broad industrial interest is represented by the manipulation of Deformable Linear Objects (DLOs), such as ropes, electric wires and cables, hoses and so on. Several literature works addressed the modeling and the manipulation of this kind of objects for several purposes and several different models and strategies were developed. A geometrically consistent model of DLOs is developed in [8] and adopted to perform numerical simulations on the object motion under gravity and during the interaction with the environment. In [9] a manipulation controller for an industrial robot inserting a cable on a tight hole without a priori knowledge of the cable parameters is proposed. The integration of robotic vision and tactile sensing for switchgear cabling tasks is presented in [10], while in [11] a vision-based rope manipulation combining self-supervised learning and imitation is proposed.

To enable that kind of DLOs modelling and manipulation, the estimation of the object parameters plays a relevant role, since the quality of the simulation and behavior prediction mostly depends on them.

[a]Department of Engineering of the University of Campania "Luigi Vanvitelli", Via Roma 29 - 81031, Aversa (CE), Italy.

[b]Department of Electrical, Electronic and Information Engineering "Guglielmo Marconi" (DEI) of the University of Bologna, Italy.

The research leading to these results has received funding from the EC Horizon 2020 research and innovation program under grant agreement n. 870133, correspondent to the project entitled REMODEL, Robotic Technologies for the Manipulation of Complex Deformable Linear objects

Corresponding author: *gianluca.palli@unibo.it*

II. Dynamic Model of DLOs

A. DLO Configuration and Lagrange Equation

The DLO model can be represented by a 3-rd order spline basis as a function of a free coordinate u representing the position along the cable starting from an end point, where $u = 0$, to the opposite end where $u = L$, being L the length of the cable

$$q(u) = \sum_{i=1}^{n_u} b_i(u) q_i \tag{1}$$

where $q(u) = (x(u),\, y(u),\, z(u),\, \theta(u)) = (r(u), \theta(u))$ is the 4-th dimensional configuration functional space of the cable, including three linear coordinates x, y, z of the DLO position at point u and the axial DLO twisting θ, $b_i(u)$ is the i-th elements of the spline polynomial basis used to represent the DLO shape and q_i are n_u properly selected coefficients, usually called *control points*, used to interpolate the DLO shape through the $b_i(u)$ function basis. This mathematical model of DLO is very effective for a number of reasons. First, the computation of the shape spatial derivatives is straightforward, i.e.

$$q'(u) = \sum_{i=1}^{n_u} b_i'(u) q_i, \quad q''(u) = \sum_{i=1}^{n_u} b_i''(u) q_i \tag{2}$$

and, most notably, can be represented through the same coefficients and simple-to-compute derivatives of the polynomial spline basis functions $b_i(u)$. Second, the proprieties of spline basis ensures minimization of the DLO model curvature. Third, this model allows to represent a generic nonlinear function with sufficient smoothness properties as a linear combination of the nonlinear function basis $b_i(u)$, that depend only on the free variable u, by the linear coefficients q_i.

The dynamic model of the DLO can be defined as a function of the control points q_i by referring to the Lagrange equations of the system

$$\frac{d}{dt}\left(\frac{\partial T}{\partial \dot{q}_i}\right) = F_i - \frac{\partial U}{\partial q_i}, \quad \forall i \in \{1, \ldots, n_u\} \tag{3}$$

where F_i is the resultant external force acting on the i-th control point, T is the overall kinetic energy of the system and U is the overall potential energy due to gravity, stretching, bending and torsional effects acting on the DLO.

B. DLO Kinetic Energy and Inertial Force

The kinetic energy of the DLO is due to translation of the control points and rotation of the cross sections. The overall

kinetic energy can be represented as a function of the control points q_i as

$$T = \frac{1}{2}\int_0^L \frac{dq^T}{dt} J \frac{dq}{dt} ds, \quad J = \begin{bmatrix} \mu & 0 & 0 & 0 \\ 0 & \mu & 0 & 0 \\ 0 & 0 & \mu & 0 \\ 0 & 0 & 0 & I \end{bmatrix} \tag{4}$$

where $ds = \|r'(u)\|du$ is the element displacement, J is the generalized density matrix of the DLO, μ is the linear density and I is the polar moment of inertia. Following the procedure described in [12], it is possible to write

$$\frac{d}{dt}\left(\frac{\partial T}{\partial \dot{q}_i}\right) = \sum_{j=1}^{n_u} J \int_0^L b_i(s) b_j(s) ds \, \frac{d^2 q_j}{dt^2} \tag{5}$$

By considering that $\frac{d^2 q_j}{dt^2} = A_j$ is the acceleration of the j-th control point, the term $J\int_0^L b_i(s)b_j(s)ds = M_{ij}$ can be considered the corresponding inertia term. Therefore, it is possible to write

$$\frac{d}{dt}\left(\frac{\partial T}{\partial \dot{q}_i}\right) = \sum_{j=1}^{n_u} M_{ij}\ddot{q}_j \tag{6}$$

and, extending this definition to the whole system, this allows to write the overall DLO inertial forces as $M\ddot{q}$, where M is the DLO inertia matrix and $\ddot{q}$ is the vector of the control point accelerations.

C. DLO Potential Energy and Elastic Forces

The potential energy U is composed by the gravity effect and the strain energy. While the derivation of the gravitational energy is quite straightforward, the strain energy can be defined by introducing the strain vector $\epsilon = [\epsilon_s, \ \epsilon_b, \ \epsilon_t]$, where $\epsilon_s = 1 - \|r'\|$, $\epsilon_t = \theta' - \tau$, $\epsilon_b = \frac{\|\mathcal{C}\|}{\|r'\|^3}$ are the stretching, the bending and the torsional term respectively and $\mathcal{C} = r' \times r''$, $\tau = \frac{\mathcal{C}^T r'''}{\|\mathcal{C}\|^2}$. It follows that the strain energy can be written as

$$U = \frac{1}{2}\int_0^L (\epsilon - \epsilon_0)^T H (\epsilon - \epsilon_0) ds = \frac{1}{2}\int_0^L \epsilon_e^T H \epsilon_e ds \tag{7}$$

where

$$H = \frac{D^2\pi}{4}\begin{bmatrix} E & 0 & 0 \\ 0 & \frac{GD^2}{8} & 0 \\ 0 & 0 & \frac{ED^2}{16} \end{bmatrix}$$

is the element stiffness matrix, E and G are the Young modulus and the shear modulus of the material respectively, D is the DLO cross section diameter and ϵ_0 is the plastic strain, or *strain memory*, of the DLO, that allows to take into account the plasticity of the material, and $\epsilon_e = \epsilon - \epsilon_0$ is the residual strain. The right side term of eq. (3) can be written as

$$P_i = -\frac{\partial U}{\partial q_i} = -\frac{1}{2}\int_0^L \frac{\partial \epsilon_e^T H \epsilon_e}{\partial q_i} ds = -\int_0^L \frac{\partial \epsilon}{\partial q_i}^T H \epsilon_e ds \tag{8}$$

representing the elastic forces due to the DLO deformation. Additional details on the DLO modeling can be found in [13].

D. DLO Dynamic Model

By extending eqs. (3), (6) and (8) to all the control points, it is possible to write the overall DLO dynamic model as

$$M\ddot{q} + N\dot{q} = F + P \tag{9}$$

where the term $N\dot{q}$ is introduced in order to take into account for DLO internal energy dissipation, F is the vector of all the external forces, gravity included, and P is the vector of all the elastic forces.

III. Numerical-Experimental Verification

The choice of model parameters is fundamental, and since no *a priori* knowledge of these parameters exists, it is necessary to estimate them through an experimental procedure. In this paper, a first procedure based on a trial and error technique, exploiting a vision based approach through a calibrated camera, is proposed to compare a simulated and an actual one, starting from different initial configurations, and under different constraints. An additional objective is also to find DLO configurations that better highlight the dependence of the shape on the physical parameters.

A. Estimation process

Given a real DLO, the objective is to estimate its mechanical parameters which allow to well describe the DLO through the proposed model. While parameters as diameter and length can be clearly fixed, other parameters are completely unknown. The objective is to correlate the model and the real DLO by experimentally estimating the best values of Young's modulus E and volume density μ, which are the parameters that most modify the behavior of the simulated DLO. During the experiments all other parameters are considered known and fixed. The parameter estimation process is based on the comparison between the shape obtained by subjecting the real DLO to a certain manipulation operation, and the shape obtained by considering the same operations on a simulated DLO. Different configurations are considered for the comparison, in order to obtain the set of parameters (E, μ), that best represents the real DLO. A first set of configurations is used to estimate and to refine the parameters and a second set (with different configurations) is used to validate estimated (E, μ).

To perform the matching between the two shapes, a calibrated camera is used. First of all, since the real DLO has to be simulated, the control points have to be chosen. An easy way is to choose these points directly on the image, by selecting a set of point on the DLO. By using the calibration information, the pixel positions can be converted into camera or world frame points. Once the initial control points are chosen, the model can be used to simulate the DLO dynamics, by imposing the same constraints, and the same setup of the real DLO. Finally, by projecting on the image plane the final B-spline obtained, the two shape can be compared. Although a first feedback can be obtained qualitatively, by evaluating the matching between the two shapes directly on the image, for a quantitative evaluation a function that represents the error committed between the real and the simulated shape has to

be defined. In order to define the error function, comparable quantities are needed, so using the same vision based approach used to choose the initial control points, an optimal B-Spline can be obtained by choosing the control points that best fit the real shape on the image. Let denote this B-Spline as $q_{\text{des}}(u)$, by indicating this as the desired final shape, and denote as $q(u)$ the B-Spline obtained from the simulation. Note that the generic B-Spline, provided by the model, is a four coordinates B-Spline, while from the image only two coordinates can be obtained. However the reported experiments involve only two components, so that the two splines are comparable. Hence, the following synthetic indicator, representing the overall error along the spline, can be defined

$$ERR = \frac{1}{L}\int_u || \, q_{\text{des}}(u) - q(u)||du \tag{10}$$

with $u \in [0, L]$, where L is the DLO length. Once an error indicator is defined, the best model parameters (E, μ) are selected by minimizing the indicator. In this work, the parameters selection is made by carrying out a set of simulation with a trial and error approach, by varying the Young modulus and the volume density, and by comparing the results with the real shape on the basis of obtained error. The DLO configuration used to obtain the parameters have to be chosen accurately: for simple configurations, a large range of parameters well reproduce the dynamics with low errors, but by considering complex configuration, this is not true anymore, so that a specific set can be identified.

B. Experimental setup

The experimental setup consists of a pre-drilled extruded polystyrene sheet, an RGB camera, some nylon ropes of different diameters and available in several lengths. Since the holes are at a predetermined distance, the polystyrene sheet is used to precisely fix the constraints imposed on the DLO, sticking a pointed object between the rope and the hole. An example of the ropes used in the experiments are shown in Fig. 1a, with the diameter equal to $4\,$mm and $8\,$mm respectively. For all experiments described in the following sections, the sheet is vertically mounted so that the used ropes are subjected only to the gravity. The friction among polystyrene sheet and ropes is considered negligible with respect to the gravity effects. The used camera is a standard RGB camera with 1920×1080 resolution. Accurate knowledge of the camera intrinsic and extrinsic parameters is essential to use the camera for quantitative geometric measurements, and in particular as reference measurement system for DLO shape. The actual parameters depends on several technical elements and they are not usually provided by manufacturers. The camera calibration allows to estimate all needed parameters and there exist several calibration techniques. In this paper, the *Camera Calibrator App*, from the Computer Vision Toolbox of MATLAB, implementing the algorithm provided in [14], is used. It exploits multiple views, from unknown position and orientation in space, of the same pattern (reported in Fig. 1b) of known structure and dimensions.

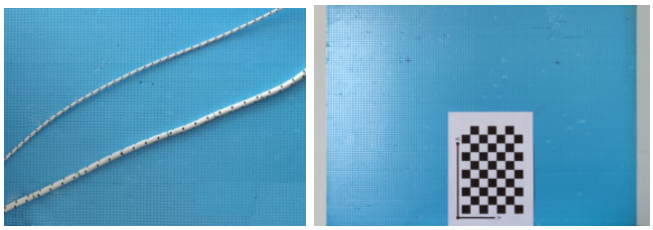

(a) (b)

Fig. 1. The polystyrene sheet and two ropes with diameter equal to $4\,$mm and $8\,$mm, respectively (a) and the pattern, collocated on the sheet, to calibrate the camera (b).

C. First Experiment: a simple configuration

The DLO used for this first experiment is a nylon rope with a diameter $D = 4\,$mm and a length $L = 0.4\,$m. The considered starting configuration of the rope is the one reported in Fig. 2a. The same figure show the initial control points, directly chosen from the image by using the vision based approach. These control points, used for the simulation, correspond to the initial B-spline reported on the same figure. The rope is initially stationary, which corresponds to null velocities and accelerations as initial conditions. By comparing initial and final configurations in Fig. 2 is is evident that the first two control points are fixed and hence, they have to be considered as constrains. Moreover, Fig. 2b shows the final DLO shape, obtained by imposing a linear trajectory on the last control point. By using the pre-drilled holes, the final shape can be accurately acquired by using the vision system, and, compared with the initial shape, it also allows to acquire the linear trajectory applied on the last control point. All data acquired from the images (e.g., control points positions, trajectories) can be converted into 3D data points by using the camera calibration parameters, previously estimated. The 3D data together with the model parameters reported in Table I are used to simulate the rope with the same initial conditions and constrains fixed for the real rope. Note that the Young's modulus E and the shear modulus G, used in the model, are interrelated by the formula $G = E/[2(1 + \nu)]$, incorporating the Poisson's ratio, which is considered constant to the value $\nu = 0.33$ in all following simulations. The model parameters selected for this first experiment are chosen on the basis of the known information about the rope material. Several frames taken from the simulation can be compared with the real final configuration in order to evaluate if indeed and in how much time the model converges towards the real final shape, with the selected model parameters. Figure 3 shows some frames from the simulation, superimposed on the camera view of the final DLO shape. The simulation lasts $3\,$s, and the trajectory is applied to the final control point during the first $1.5\,$s, so that in the second part of the simulation (from $t = 1.5\,$s to $t = 3\,$s) the last control point position is fixed, and the gravity force is the only external force acting on the rope. By comparing the final simulation frame with the real shape, see Fig. 3d, it is evident that the selected parameters allows an accurate modelling for the considered DLO. This good result

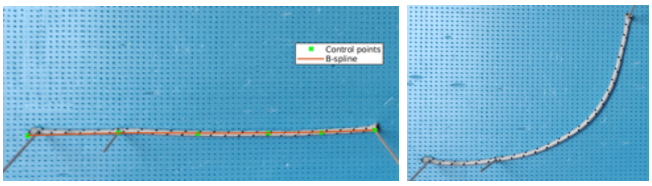

(a) (b)

Fig. 2. First experiment: initial configuration with control points (a) and final configuration (b).

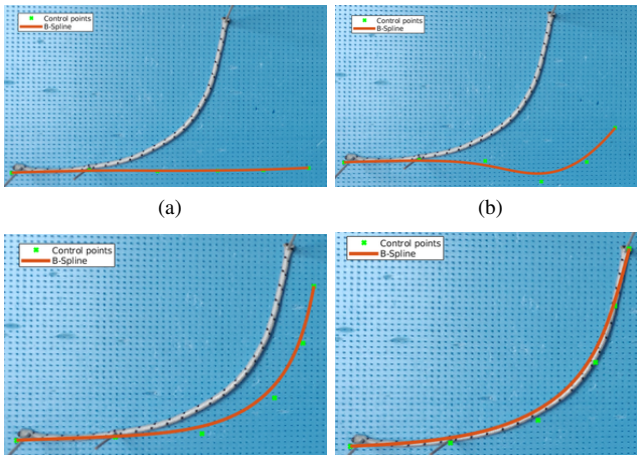

(a) (b)

(c) (d)

Fig. 3. First experiment: comparison of simulation frames at the time instants $t = 0\,\text{s}$ (a), $t = 0.5\,\text{s}$ (b), $t = 1\,\text{s}$ (c), $t = 3\,\text{s}$ (d) with the real final configuration.

also depends on the simple considered configuration, for which variations in the mechanical parameters of the DLO do not have much effect. As a consequence, additional considerations are needed with more complex configurations. In order to quantify the correlation between the model and the real rope, the synthetic indicator in Eq. (10) is computed by comparing the real final shape, acquired from the vision system, and the shape obtained from the model at the simulation end, i.e., at $t = 3\,\text{s}$., by obtaining the value $ERR = 0.069$ (corresponding to the case reported in Fig. 3d).

D. Second experiment: evaluation on a different shape

The same rope is used starting from the same initial conditions and the same constraints on first two control points described in the first experiment (see Fig. 4a). In this case only the linear trajectory, applied to the last control point, is changed to reach the different final configuration reported in Fig. 4b. In this case, the DLO parameters of the first experiment do not allow to reach good performance in terms of shape reproduction. Hence, a refinement was necessary in order to properly reproduce the actual shape. In particular, the

TABLE I
DLO SIMULATION PARAMETERS FOR THE FIRST EXPERIMENT.

Parameter	E	μ	L	D
Value	1e6	2000	0.4	0.004
Unit	Pa	kg/m^3	m	m

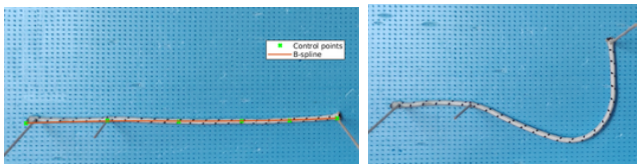

(a) (b)

Fig. 4. Second experiment: initial configuration with control points (a) and final configuration (b).

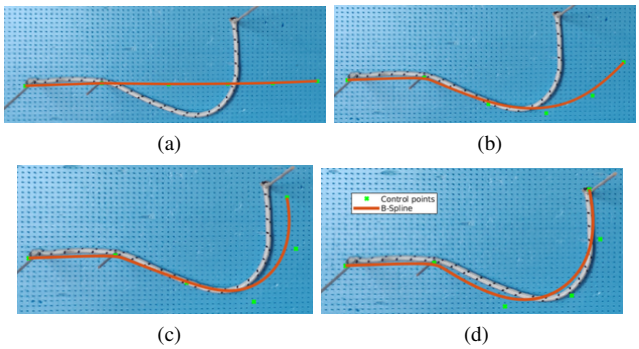

(a) (b)

(c) (d)

Fig. 5. Second experiment: comparison of simulation frames at the time instants $t = 0\,\text{s}$ (a), $t = 0.5\,\text{s}$ (b), $t = 1\,\text{s}$ (c), $t = 3\,\text{s}$ (d) with the real final configuration.

Young's modulus is increased with respect to the previous one in order to reach a good value for the synthetic indicator ERR (comparable to first experiment). The set, selected to reach a good value for the synthetic indicator ERR (comparable to first experiment), is reported in the Table II.

Figure 5 reports some frames from the simulation, superimposing on the final shape image, in order to demonstrate how with the selected parameters a correct reconstruction of DLO shape is possible. The synthetic indicator for this experiment is $ERR = 0.080$ (corresponding to the case reported in Fig. 5d), by showing a matching comparable with respect to the first experiment, but with a different value of Young's modulus.

E. Third experiment: "C" shape

The following is an experiment analogous to the previous ones (starting from the same conditions in Fig. 4a), but the final configuration is more significant for the identification of rope physical characteristics, due to its particularly "C" shape (see Fig. 6b). It is intuitive to understand how this configuration cannot be obtained with a very high range of parameters like the previous ones, since in this case the stiffness plays a key role in the shape assumed in the final instant by the DLO. As a consequence, several simulations are computed by varying the (E, μ) values in order to obtain a final shape as close as possible to the real one and with a corresponding synthetic indicator similar to previous ones.

TABLE II
DLO SIMULATION PARAMETERS FOR THE SECOND EXPERIMENT.

Parameter	E	μ	L	D
Value	3e6	2000	0.4	0.004
Unit	Pa	kg/m^3	m	m

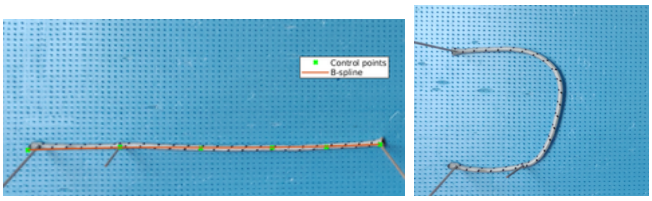

(a) (b)

Fig. 6. Third experiment: initial configuration with control points (a) and final configuration (b).

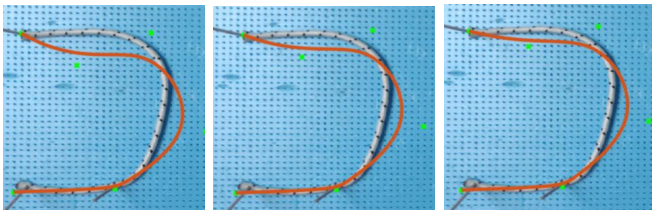

(a) (b) (c)

Fig. 7. Third experiment: comparison of simulation frames at the time instants $t = 3\,\mathrm{s}$ for different values of Young's modulus: $E = 1e6\,\mathrm{Pa}$ (a), $E = 3e6\,\mathrm{Pa}$ (b), $E = 5e7\,\mathrm{Pa}$ (c).

Figure 7 shows a set of the final instant for three different simulations, where for each picture the Young's modulus was changed, by increasing from $E = 1\mathrm{e}6\,\mathrm{Pa}$ in Fig. 7a to $E = 5\mathrm{e}7\,\mathrm{Pa}$ in Fig. 7c, while the density is increased to the value $\mu = 2500\,kg/m^3$.

It is evident that the best reconstruction corresponds to Fig. 7c, where the E value is very different from the previous experiments. Figure 7c corresponds to a simulation with the parameters in Table III and the computed synthetic indicator is $ERR = 0.092$. For the other two cases in Fig. 7a and Fig. 7b the synthetic indicator is $ERR = 0.153$ and $ERR = 0.107$, respectively.

F. Cross validation among the three experiments

The objective remains to obtain a unique set of parameters usable for the selected DLO in all cases. The set of parameters used for the more complex configuration (the last one) should be the best choice, by considering that the particular shape well depends on the physical parameters (E, μ) that have to be identify. To verify this, the values last set of identified parameters in third experiment and reported in Table III is used to reproduce the rope dynamics in first two experiments. Hence, all the simulations are repeated by using the last parameters. From the obtained shape point of view there are not evident differences with respect to the results already presented in Fig. 3d and Fig. 5d. The quality of the last parameters can be quantitatively evaluated by comparing the synthetic indicator computed by using the set in Table III with the sets in Table I and Table II, respectively. Table IV summarizes the synthetic indicator for all experiments and parameters values, by highlighting how the last set in Table III guarantees the best reconstruction for all cases, and hence can be selected as physical parameters for the considered DLO.

TABLE III
DLO SIMULATION PARAMETERS FOR THE THIRD EXPERIMENT.

Parameter	E	μ	L	D
Value	5e7	2500	0.4	0.004
Unit	Pa	kg/m^3	m	m

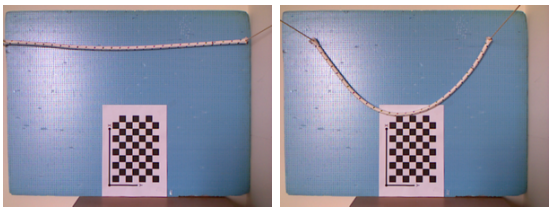

(a) (b)

Fig. 8. First validation experiment: initial configuration (a) and final configuration (b).

IV. VALIDATION EXPERIMENTS

The physical parameters estimated in the previous section are used with a different rope of the same material, in order to validate in separate experiments the estimation quality. In particular, a rope of the same material but with a length $L = 0.8\,\mathrm{m}$ and a diameter $D = 8\,\mathrm{mm}$ is used. Hence, the parameters used for the simulations are the ones reported in Table V.

Figure 8a shows the initial DLO configuration, where the DLO is fixed at the two ends, on the polystyrene sheet under the gravity effects. The experiment consist of imposing a trajectory on the first and the last control points (DLO ends), making them approaching to the center by maintaining constant the z-coordinate. When the trajectory is accomplished, the two points have to remain constrained at the final position, while the rope is affected only by the gravity. The whole simulation lasts 2 s, and the trajectory is applied to the DLO ends during the first 1 s, so that in the second part of the simulation (from $t = 1\,\mathrm{s}$ to $t = 2\,\mathrm{s}$) the DLO ends position are fixed, and the gravity force is the only external force acting on the rope. The reached final configuration is the one reported in Fig. 8b. Figure 9 shows some frames from the simulation, superimposed on the camera view of the final DLO shape. The dynamics obtained is quite realistic, and from a vision comparison, the final shape is reproduced very well by this simulation (see Fig. 9d). Also the computed synthetic indicator $ERR = 0.068$ confirms the quality of the reconstructed shape.

TABLE IV
COMPARISON OF THE THREE EXPERIMENTS BY USING ERR INDICATOR.

	First exp.		Second exp.		Third exp.		
E	1e6	5e7	3e6	5e7	1e6	3e6	5e7
μ	2000	2500	2000	2500	2000	2000	2500
ERR	0.069	0.067	0.080	0.077	0.153	0.107	0.092

TABLE V
DLO SIMULATION PARAMETERS FOR THE VALIDATION EXPERIMENTS.

Parameter	E	μ	L	D
Value	5e7	2500	0.8	0.008
Unit	Pa	kg/m^3	m	m

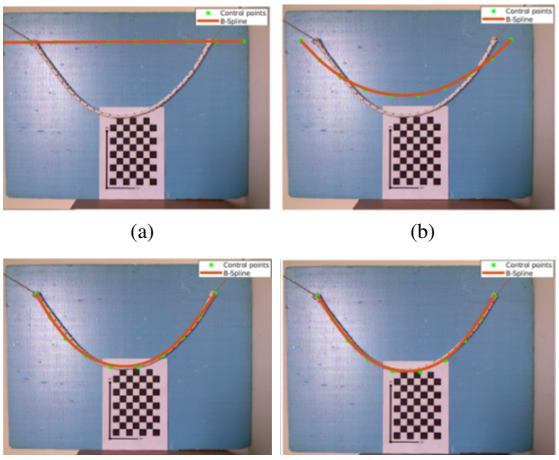

(a) (b) (c) (d)

Fig. 9. First validation experiment: comparison of simulation frames at the time instants $t = 0\,\text{s}$ (a), $t = 0.5\,\text{s}$ (b), $t = 1\,\text{s}$ (c), $t = 2\,\text{s}$ (d) with the real final configuration.

A second validation experiment is implemented, starting from the same initial condition of the previous one, but with a final shape more complex, reported in Fig. 10b. In this case the final shape present four imposed constraints: the first two control points on the left, and last two on the right, (Control point 1, Control point 2, Control point 9, Control point 10), have to approach the center by maintaining constant their z-coordinates. The elastic DLO properties have a fundamental role in the final shape. This can be a further demonstration that the chosen parameters are very good. The simulation is performed in the same time and only the final frame is reported in Fig. 11. The reconstruction quality is still similar to previous ones with a synthetic indicator $ERR = 0.090$. A video attached to the paper shows the superimposition of the simulation and the final shape for all considered experiments.

V. Conclusions

In this paper a first numerical-experimental correlation of the proposed model for DLOs is presented. The main objective was the estimation of physical parameters for the considered DLOs, which allow to return the simulated rope shapes that best approximate the real ones. A second objective was to detect the best configuration that allow the parameters identification. With a trial and error approach and a continuous refinement the values $E = 5\text{e}7\,\text{Pa}$ and $\mu = 2500\,kg/m^3$ are identify on a first set of experiment made on a rope with length $L = 0.4\,\text{m}$ and diameter $D = 4\,\text{mm}$. Validation experiments made on a rope with length $L = 0.8\,\text{m}$ and diameter $D = 8\,\text{mm}$ are used to verify the identified parameters. In future developments an automatic optimization procedure will be implemented, by minimizing the synthetic indicator here defined and used to quantify the quality of shape reconstructions.

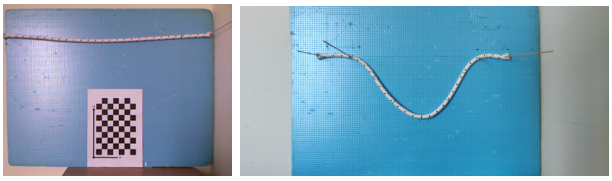

(a) (b)

Fig. 10. Second validation experiment: initial configuration (a) and final configuration (b).

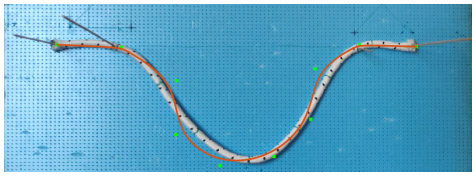

Fig. 11. Second validation experiment: comparison of simulated and real shape.

References

[1] R. J. Moreno Masey, J. O. Gray, T. J. Dodd, and D. G. Caldwell, "Guidelines for the design of low-cost robots for the food industry," *Industrial Robot: An International Journal*, vol. 37, no. 6, pp. 509–517, 2010.

[2] A. Ramisa, G. Alenya, F. Moreno-Noguer, and C. Torras, "Using depth and appearance features for informed robot grasping of highly wrinkled clothes," in *Proc. IEEE Int. Conf. on Robotics and Automation*, 2012, pp. 1703–1708.

[3] J. Pile, G. B. Wanna, and N. Simaan, "Force-based flexible path plans for robotic electrode insertion," in *Proc. IEEE Int. Conf. on Robotics and Automation*, 2014, pp. 297–303.

[4] X. Jiang, K.-m. Koo, K. Kikuchi, A. Konno, and M. Uchiyama, "Robotized assembly of a wire harness in a car production line," *Advanced Robotics*, vol. 25, no. 3-4, pp. 473–489, 2011.

[5] A. Shah, L. Blumberg, and J. Shah, "Planning for manipulation of interlinked deformable linear objects with applications to aircraft assembly," *IEEE Tran. on Automation Science and Engineering*, vol. 15, no. 4, pp. 1823–1838, 2018.

[6] T. Hermansson, R. Bohlin, J. S. Carlson, and R. Söderberg, "Automatic assembly path planning for wiring harness installations," *Journal of manufacturing systems*, vol. 32, no. 3, pp. 417–422, 2013.

[7] J. Sanchez, J.-A. Corrales, B.-C. Bouzgarrou, and Y. Mezouar, "Robotic manipulation and sensing of deformable objects in domestic and industrial applications: a survey," *The Int. J. of Robotics Research*, vol. 37, no. 7, pp. 688–716, 2018.

[8] A. Theetten, L. Grisoni, C. Andriot, and B. Barsky, "Geometrically exact dynamic splines," *Computer-Aided Design*, vol. 40, no. 1, pp. 35 – 48, 2008.

[9] R. Zanella, D. De Gregorio, S. Pirozzi, and G. Palli, "Dlo-in-hole for assembly tasks with tactile feedback and lstm networks," in *Proc. Int. Conf. on Control, Decision and Information Technologies (CoDIT)*, 2019, pp. 285–290.

[10] D. De Gregorio, R. Zanella, G. Palli, S. Pirozzi, and C. Melchiorri, "Integration of robotic vision and tactile sensing for wire-terminal insertion tasks," *IEEE Tran. on Automation Science and Engineering*, vol. 16, no. 2, pp. 585–598, 2018.

[11] A. Nair, D. Chen, P. Agrawal, P. Isola, P. Abbeel, J. Malik, and S. Levine, "Combining self-supervised learning and imitation for vision-based rope manipulation," in *Proc. IEEE Int. Conf. on Robotics and Automation*, 2017, pp. 2146–2153.

[12] O. Nocent and Y. Remion, "Continuous deformation energy for dynamic material splines subject to finite displacements," in *Computer Animation and Simulation 2001*, N. Magnenat-Thalmann and D. Thalmann, Eds. Vienna: Springer Vienna, 2001, pp. 87–97.

[13] G. Palli, "Model-based manipulation of deformable linear objects by multivariate dynamic splines," in *Proc. IEEE Int. Conf. on Industrial Cyberphysical Systems*, 2020, pp. 520–525.

[14] W. Burger, "Zhang's camera calibration algorithm: In-depth tutorial and implementation," University of Applied Sciences Upper Austria, School of Informatics, Communications and Media, Dept. of Digital Media, Hagenberg, Austria, Tech. Rep. HGB16-05, May 2016.